Polarized γ-photon beams produced by collision of two ultrarelativistic electron beams

Zhe Gao[1,2] and Wei-Min Wang[1,2,3,*]

[1]*Department of Physics and Beijing Key Laboratory of Opto-electronic Functional Materials and Micro-nano Devices, Renmin University of China, Beijing 100872, China*

[2]*Key Laboratory of Quantum State Construction and Manipulation (Ministry of Education), Renmin University of China, Beijing 100872, China*

[3]*IFSA Collaborative Innovation Center, Shanghai Jiao Tong University, Shanghai 200240, China*

(Received 25 October 2023; revised 8 April 2024; accepted 7 June 2024; published 3 July 2024)

Many studies have shown that high-energy γ-photon beams can be efficiently generated via nonlinear Compton scattering driven by laser pulses with intensities greater than 10^{22} W/cm^2 recently available in laboratories. Here we propose a laserless scheme to efficiently generate high-energy polarized γ-photon beams by collision of two ultrarelativistic electron beams. The self-generated field of a dense driving electron beam provides a strong deflection field for the other ultrarelativistic seeding electron beam. A QED Monte Carlo code based on the locally constant field approximation is employed to simulate the collision process, and the polarization properties of the γ photons produced are investigated. The simulation results and theoretical analysis indicate that the photon polarization, including both linear and circular polarizations, can be tuned by changing the initial polarization of the seeding beam. If an unpolarized seeding beam is used, linearly polarized photons with an average polarization of 55% can be obtained. If the seeding beam is transversely (longitudinally) polarized, the linear (circular) polarization of photons above 3 GeV can reach 90% (67%), which is favorable for highly polarized, high-energy γ-photon sources.

DOI: 10.1103/PhysRevA.110.013502

I. INTRODUCTION

Polarized γ-photon beams play an important role in astrophysics [1], nuclear physics [2], high-energy physics [3,4], and plasma physics [5]. For example, in high-energy physics, the linearly polarized photon beam can be used to distinguish Delbrück scattering from other elastic scattering processes [4] and achieve a more accurate measurement of Delbrück scattering. Polarized electrons and positrons can be used to detect nuclear structures accurately [6] and verify standard models [3] in future electron-positron colliders, where traditionally the circularly polarized γ-photon beams are usually needed to generate these polarized positrons via the Bethe-Heitler process.

Polarized γ photons can be obtained through Compton scattering [7–9] and bremsstrahlung [10,11]. Unpolarized electrons can radiate polarized photons by linear Compton scattering. In linear Compton scattering, the polarization of the laser can be transferred to the polarization of the scattered photons, since the formation length of the photons is greater than the laser wavelength [12]. By contrast, the radiation formation length is smaller than the laser wavelength in nonlinear Compton scattering [13–17] and the polarization of the laser does not determine the polarization of the photon, e.g., electrons with longitudinal spin are required in producing circularly polarized photons through nonlinear Compton scattering, as will be shown in our results presented in the following. For bremsstrahlung, the polarization can be transferred from electrons to photons, but the incident electron density should be low enough to avoid the crystal being damaged [18].

With the rapid development of ultrashort, ultraintense laser technology, peak intensities of 10^{22} W/cm^2 and even 10^{23} W/cm^2 can be delivered from petawatt-level laser facilities [19,20]. By use of such laser pulses, many schemes are proposed to generate high-energy γ photons with high brightness [21,22] or certain polarization [12,15,16]. Tang *et al.* [12] showed that circularly polarized photons with a polarization of 78% or linearly polarized photons with a polarization of 91% can be obtained by using the interaction of circularly polarized or linearly polarized lasers with electrons in the weakly nonlinear Compton scattering regime. Li *et al.* [16] found that polarized γ photons can be emitted by ultrarelativistic prepolarized electrons through nonlinear Compton scattering, where the polarization of high-energy photons is determined by the electron polarization. Xue *et al.* [15] proposed to generate polarized γ photons by intense laser interaction with plasmas, for which the photon brilliance can reach 10^{21} photons /(s mm^2 mrad^2 0.1% BW).

Different from the laser-electron collisions or laser-plasma interactions, here we propose a laserless scheme to generate polarized γ-photon beams via the collision of two ultrarelativistic electron beams [23,24]. In the proposed scheme, one electron beam is the driving beam and the other is the seeding beam. The driving beam can provide a strong self-generated field, which plays a role similar to the laser field in the conventional nonlinear Compton scattering scheme.

*Contact author: weiminwang1@ruc.edu.cn

The self-generated azimuthal magnetic field is perpendicular to the radial electric field, under which the seeding beam can experience transverse Lorentz force and strongly emit γ photons. Our simulation results show that if an unpolarized seeding beam is used, linearly polarized photon beams with an average polarization of 55% can be generated. Because the field experienced by the seeding beam is at the same polarity, one can control the initial polarization of the seeding beam to adjust the photon polarization to be either linear or circular. The polarity of the field is important to achieve high polarization of photons. A crossed oscillating field changes the polarity with time and the direction of acceleration of the electrons also changes. To obtain photons with higher linear polarization, we take polarized electron beams whose spin direction and transverse acceleration field are opposite. Then the linear polarization of the produced high-energy photons is parallel to the $(\vec{a}_\perp, \vec{v})$ plane. While the electron spin direction is the same as the transverse acceleration field, the linear polarization of the high-energy photons is perpendicular to the $(\vec{a}_\perp, \vec{v})$ plane. In this case, if a crossed oscillating field is adopted, the acceleration field is alternating to be the same and opposite to the electron spin direction, which causes the linear polarization of the produced high-energy photons to alternate between parallel and perpendicular to the $(\vec{a}_\perp, \vec{v})$ plane. Then the linear polarization of the high-energy photons tends to be small. Otherwise, the linear polarization of the produced photons is always parallel to the $(\vec{a}_\perp, \vec{v})$ plane if the field experienced by the seeding beam is at the same polarity.

II. THEORETICAL MODEL

In this work we use the collision of two ultrarelativistic electron beams to produce polarized γ photons, one of which is the seeding beam and the other is the driving beam. The driving beam provides a superstrong self-generated field. We take the charge density of the driving beam as a Gaussian distribution, i.e., $\rho = \rho_0 e^{-r^2/2\sigma_d^2} e^{-(z-z_0-vt)^2/2l_d^2}$, where $\rho_0 = \frac{Q_d}{(2\pi)^{3/2}\sigma_d^2 l_d}$ is the maximum value of the charge density (with Q_d, l_d, and σ_d the total charge, bunch length, and bunch width, respectively), z_0 is the initial center position of the driving beam, and $r = \sqrt{x^2+y^2}$. In the ultrarelativistic case, the self-generated field of the driving beam is approximately $E_r(r,z,t) \approx B_\theta(r,z,t) \approx 4\pi\rho_0 \frac{\sigma_d^2}{r}(1 - e^{-r^2/2\sigma_d^2}) e^{-(z-z_0-vt)^2/2l_d^2}$ [25,26]. There is a maximum field strength $B_\theta^{\max}$ at $r \approx 1.585\sigma_d$ and $z = z_0 + vt$, where

$$B_\theta^{\max} \approx 1.08 \times 10^4 \times \frac{Q_d\ (\mathrm{nC})}{\sigma_d\ (\mu\mathrm{m}) \times l_d\ (\mu\mathrm{m})}. \tag{1}$$

The longitudinal field components $E_z(r,z,t)$ and $B_z(r,z,t)$ can be negligible. The maximum value of the QED parameter is about

$$\chi_e^{\max} \approx 0.0096 \times \frac{Q_d\ (\mathrm{nC}) \times \varepsilon_{s0}\ (\mathrm{GeV})}{\sigma_d\ (\mu\mathrm{m}) \times l_d\ (\mu\mathrm{m})}, \tag{2}$$

where ε_{s0} is the initial electron energy of the seeding beam.

In this article, a Monte Carlo algorithm is used to simulate the polarized photon emission [27–29]. The spin flip of electrons due to radiative polarization and the determination of photon polarization are included [16,30,31]. This code has been used in the previous work to investigate polarized pair production [32]. We use the spin- and polarization-resolved photon radiation probability derived from the semiclassical QED operator method [13,16,30,33,34], where the local constant field approximation (LCFA) [35–39] is used. If the external field satisfies $a_0 = \frac{|e|E}{m_e c\omega_0} \gg 1$, it is generally considered to satisfy the LCFA, where a_0 is the normalized field strength, ω_0 is the laser frequency, and E is the deflection field strength. The angular-resolved radiation probability can be expressed as

$$\begin{aligned}\frac{d^2W_{\mathrm{rad}}}{dudt} = \frac{\alpha m^2 c^4}{2\sqrt{3}\pi\hbar\varepsilon_e}\Bigg[&\frac{u^2-2u+2}{1-u}K_{2/3}(y) \\ &- \mathrm{Int}K_{1/3}(y) - uK_{1/3}(y)(\vec{S}_i\cdot\vec{e}_2) \\ &+ \frac{u}{1-u}K_{1/3}(y)(\vec{S}_i\cdot\vec{e}_1)\xi_1 \\ &+ \left(\frac{2u-u^2}{1-u}K_{2/3}(y) - u\,\mathrm{Int}K_{1/3}(y)\right)(\vec{S}_i\cdot\vec{e}_v)\xi_2 \\ &+ \left(K_{2/3}(y) - \frac{u}{1-u}K_{1/3}(y)(\vec{S}_i\cdot\vec{e}_2)\right)\xi_3\Bigg],\end{aligned} \tag{3}$$

where $K_\nu(y)$ is the modified Bessel function of the second kind of the νth order, $y = \frac{2u}{3(1-u)\chi_e}$, $u = \frac{\varepsilon_\gamma}{\varepsilon_e}$ is the ratio of the photon energy to the electron energy, $\alpha \approx \frac{1}{137}$ is the fine-structure constant, and $\chi_e = \frac{e\hbar}{m_e^3c^4}|F_{\mu\nu}p^\nu|$ is the nonlinear quantum parameter. Physical variables e, c, m_e, $\hbar$, $F_{\mu\nu}$, and p^ν are the electron charge, the speed of light, the electron mass, the reduced Planck constant, the electromagnetic field tensor, and the electron four-dimensional momentum, respectively. Vectors $\vec{S}_i$ and $\vec{S}_f$ are the electron spin-polarization vectors before and after the emission. Here $|\vec{S}_i| = |\vec{S}_f| = 1$, which means the electron is in a pure state. Since we are mainly concerned with photon polarization, here we have summed the final states of electrons. The normalized Stokes vector $\vec{\xi} = (\xi_1, \xi_2, \xi_3)$ is used to describe the photon polarization. The Stokes vector depends on the specific coordinate system and we select $(\vec{e}_1, \vec{e}_2, \vec{e}_v)$, where $\vec{e}_1$ is the direction of the transverse acceleration of the electron, $\vec{e}_v$ is the velocity direction of the electron, and $\vec{e}_2 = \vec{e}_v \times \vec{e}_1$. The Stokes component $\xi_1 = +1$ (-1) means that the photon is linearly polarized at an angle of $\pi/4$ right to the direction $\vec{e}_1$ $(\vec{e}_2)$, $\xi_3 = +1$ (-1) means that the photon is linearly polarized along the direction $\vec{e}_1$ $(\vec{e}_2)$, and $\xi_2 = +1$ (-1) means that the photon is right-handed (left-handed) circularly polarized.

In the process of photon emission, we introduce two uniform random numbers r_1 and r_2 in the interval of (0,1). When $3r_1^2 dW_{\mathrm{total}}(u_0)/du > r_2$, a photon with an energy proportion of $u_0 = r_1^3$ is radiated [29], where W_{total} is the total radiation probability. Then we take another random number $r_3 \in (0,1)$ to determine the photon polarization. Equation (3) can be written as $\frac{dW_{\mathrm{rad}}^2}{dudt} = W_0 + W_1\xi_1 + W_2\xi_2 + W_3\xi_3 = W_0 + \vec{W}\cdot\vec{\xi} = W_0 + |\vec{W}|\hat{W}\cdot\vec{\xi}$, where $|\vec{W}| = \sqrt{W_1^2+W_2^2+W_3^2}$ and $\hat{W}$ is the direction vector of $\vec{W}$. When a photon is radiated, it collapses into a pure state along the $\hat{W}$ direction or its opposite direction. If $\frac{dW_{\mathrm{rad}}^2}{dudt}|_{\vec{\xi}=\hat{W}} / (\frac{dW_{\mathrm{rad}}^2}{dudt}|_{\vec{\xi}=\hat{W}} + \frac{dW_{\mathrm{rad}}^2}{dudt}|_{\vec{\xi}=-\hat{W}}) > r_3$, then $\vec{\xi} = \hat{W}$; otherwise $\vec{\xi} = -\hat{W}$, where $\frac{dW_{\mathrm{rad}}^2}{dudt}|_{\vec{\xi}=\hat{W}} = W_0 +$

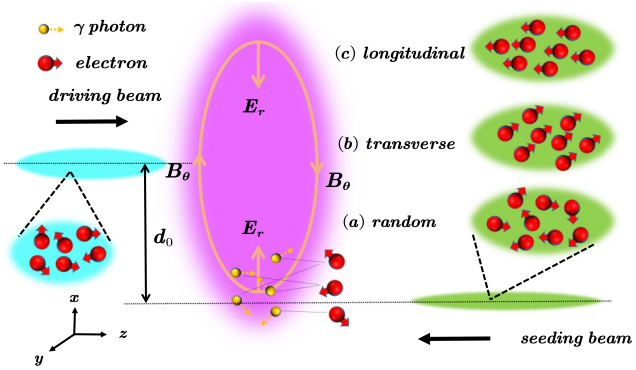

FIG. 1. Interaction scenario of an ultrarelativistic seeding electron beam colliding head-on with a dense driving electron beam. The driving beam provides a superstrong self-generated field. In such a transverse field the seeding beam emits polarized γ photons, whose emission direction is approximately along the propagation direction of the seeding beam.

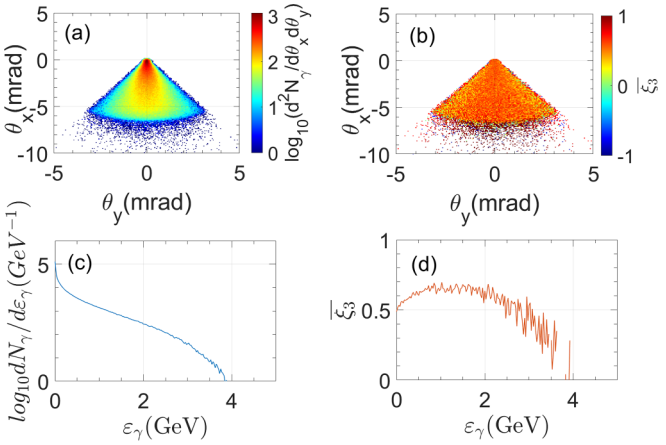

FIG. 2. (a) Photon-number density $\log_{10}(d^2N_\gamma/d\theta_x d\theta_y)$ and (b) photon polarization $\overline{\xi_3}$ versus deflection angles θ_x and θ_y, where $\theta_x \approx \frac{p_x}{|p_z|}$ and $\theta_y \approx \frac{p_y}{|p_z|}$. (c) Photon spectrum $\log_{10} dN_\gamma/d\varepsilon_\gamma$ and (d) photon polarization $\overline{\xi_3}$ versus photon energy ε_γ.

$|\vec{W}|$ and $\frac{dW^2_{\rm rad}}{dudt}|_{\vec{\xi}=-\hat{W}} = W_0 - |\vec{W}|$. After a photon is radiated, the electron spin state collapses to one of the basis states determined by the spin quantization axis (SQA). Here we choose the fixed axis $\vec{v} \times \vec{a}$ as the SQA [14,15,40], which is the magnetic-field direction of the electron in the rest coordinate system. The choice of SQA depends on the observable of interest. The spin of the electron is determined by the random number $r_4 \in (0, 1)$. If $\frac{d^2\overline{W_\gamma}}{dudt}|_{\vec{S}_f=\vec{e}_2}/(\frac{d^2\overline{W_\gamma}}{dudt}|_{\vec{S}_f=\vec{e}_2} + \frac{d^2\overline{W_\gamma}}{dudt}|_{\vec{S}_f=-\vec{e}_2}) > r_4$, then $\vec{S}_f = \vec{e}_2$; otherwise $\vec{S}_f = -\vec{e}_2$, and the derivations of $\frac{d^2\overline{W_\gamma}}{dudt}|_{\vec{S}_f=\vec{e}_2}$ and $\frac{d^2\overline{W_\gamma}}{dudt}|_{\vec{S}_f=-\vec{e}_2}$ can be found in Appendix B.

The self-generated radial field $E_r(r, z, t)$ formed by the driving beam can be considered as a half-cycle laser field with a wavelength of $4l_d$. The classical electron dynamics is described by the Newton-Lorentz force and the Thomas-Bargmann-Michel-Telegdi theory is used to describe the electron spin precession [41]. In the ultrarelativistic case, the direction of the photon emission is close to the initial electron velocity direction.

III. SIMULATION RESULTS AND ANALYSIS

A. Simulation parameters

In the typical simulation case, we take the driving electron beam with the charge $Q_d = 4$ nC, the length $l_d = 0.5$ μm, the width $\sigma_d = 1.0$ μm, and the initial energy $\varepsilon_{d0} = 10$ GeV. The seeding beam has the charge $Q_s = 0.128$ pC, the length $l_s = 1.0$ μm, the width $\sigma_s = 0.5$ μm, and the initial energy $\varepsilon_{s0} = 5$ GeV. The energy spread of the seeding beam is $\Delta\varepsilon_{s0}/\varepsilon_{s0} = 0.01$. The self-generated field of the seeding beam is 10^{-5} orders of magnitude lower than the driving beam and can be ignored. Such a driving beam and seeding beam can be provided by FACET II [42] and future laser wakefield accelerators [43]. At the initial time, the central positions of the driving beam (along the $+z$ axis) and the seeding beam (along the $-z$ axis) are (x, y, z) = (0, 0, −2 μm) and (d_0, 0, 2 μm), respectively, where d_0 is the impact parameter between two electron beams, as shown in Fig. 1. If the impact parameter of the two beams cannot be well controlled in technology, the photon polarization should average over the impact parameter and the polarization will vanish. Therefore, the control of the impact parameter is key in our case.

In our simulation, we set $\sigma_s = 0.5$ μm and $d_0 = -2$ μm to obtain efficient photon yield. Notice that when $|d_0| = 1.585\sigma_d = 1.585$ μm, χ_e is at the maximum, causing the most efficient photon yield, but the linear polarization is not the highest. As $|d_0|$ deviates from $1.585\sigma_d$ and χ_e decreases, the linear polarization increases. To balance the photon yield and the linear polarization, a moderate $|d_0|$ is required, as we have taken in our simulations. The maximum value of χ_e in the interaction is 0.38, so the QED effect needs to be taken into account. In our simulations $a_0 \approx 4 \times \frac{Q_d\ (\rm nC)}{\sigma_d\ (\mu m)} = 16 \gg 1$, ensuring that the LCFA holds.

B. Simulation results

We show the angular distributions, spectrum, and polarization of the generated photons in Fig. 2. Figure 2(a) plots the photon angular distribution with respect to θ_x and θ_y, where $\theta_x \approx \frac{p_x}{|p_z|}$ and $\theta_y \approx \frac{p_y}{|p_z|}$. The photons are mainly distributed in the small regions of -6 mrad $< \theta_x < 0$ and -0.3 mrad $< \theta_y < 0.3$ mrad. The total number of photons N_γ is about 4.1×10^5 and the energy conversion efficiency is up to $\eta = \sum_{N_\gamma} \varepsilon_\gamma / \sum_{N_s} \varepsilon_{s0} \approx 3.0\%$ [see Fig. 3(c)]. The generated photons are mainly distributed in the $-x$ direction because the Lorentz force deflects the seeding beam in the $-x$ direction. If $d_0 > 0$, the photons will be distributed in the $+x$ direction, because the self-generated field polarity is reversed. Figure 2(c) shows the distribution of photon number with photon energy and the cutoff energy of the produced photon approaches 4 GeV. When the electron charge is taken as 0.128 pC, the brilliance is 7.1×10^{15} photons /(s mm^2 mrad^2 0.1% BW) at a photon energy of 1 GeV. If the electron charge is increased to 0.2 nC, the brilliance can reach 10^{19} photons /(s mm^2 mrad^2 0.1% BW).

The produced photons are linearly polarized and the average polarization degree is about 55% [see Figs. 2(d) and

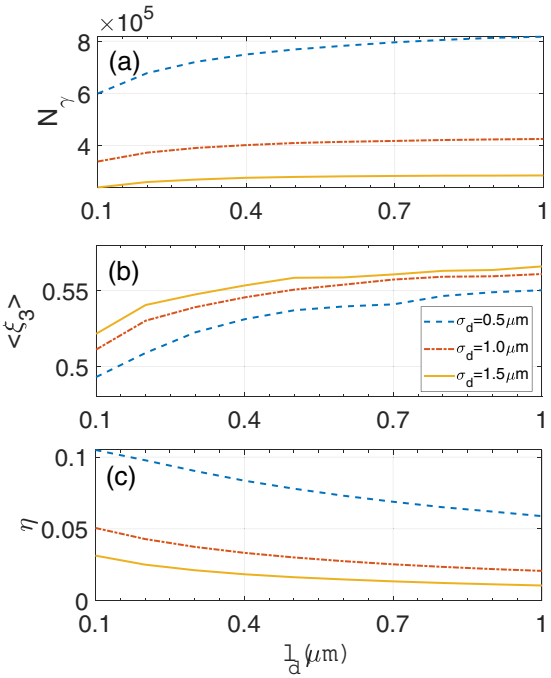

FIG. 3. (a) Photon number N_γ, (b) photon polarization $\langle\xi_3\rangle$, and (c) energy conversion efficiency η versus the driving beam length l_d in three cases with driving beam widths of $\sigma_d = 0.5$ μm (blue dashed line), 1.0 μm (orange dash-dotted line), and 1.5 μm (yellow solid line), respectively.

3(b)]. In our case $\overline{\xi_1} \approx 0$, $\overline{\xi_2} \approx 0$, and the average polarization degree is defined as $P_\gamma = \sqrt{(\overline{\xi_1})^2 + (\overline{\xi_2})^2 + (\overline{\xi_3})^2} \approx |\overline{\xi_3}|$. According to Eq. (3), the average linear polarization degree of photons can be expressed as

$$\overline{\xi_3} = \frac{K_{2/3}(y) - \frac{u}{1-u}K_{1/3}(y)(\vec{S}_i \cdot \vec{e}_2)}{\frac{u^2-2u+2}{1-u}K_{2/3}(y) - \mathrm{Int}K_{1/3}(y) - uK_{1/3}(y)(\vec{S}_i \cdot \vec{e}_2)}. \quad (4)$$

Due to the quantum effect, the photon polarization can only take the direction of parallel and antiparallel to $\hat{W}$ and the corresponding probabilities are $\frac{dW^2_{\mathrm{rad}}}{dudt}|_{\vec{\xi}=\hat{W}} = W_0 + |\vec{W}|$ and $\frac{dW^2_{\mathrm{rad}}}{dudt}|_{\vec{\xi}=-\hat{W}} = W_0 - |\vec{W}|$, respectively [34]. The corresponding probabilities are linearly superimposed and the polarization of the final photon is achieved as $(\frac{dW^2_{\mathrm{rad}}}{dudt}|_{\vec{\xi}=\hat{W}} - \frac{dW^2_{\mathrm{rad}}}{dudt}|_{\vec{\xi}=-\hat{W}})\hat{W}/(\frac{dW^2_{\mathrm{rad}}}{dudt}|_{\vec{\xi}=\hat{W}} + \frac{dW^2_{\mathrm{rad}}}{dudt}|_{\vec{\xi}=-\hat{W}}) = \vec{W}/W_0$, that is, $\overline{\xi_3} = W_3/W_0$.

In the case of the unpolarized seeding beam, the influences of spin on the polarization degree of photons cancel each other, so one can take $\vec{S}_i \cdot \vec{e}_2 = 0$. Then $\overline{\xi_3}$ can be simplified to

$$\overline{\xi_3} \approx \frac{K_{2/3}(y)}{\frac{u^2-2u+2}{1-u}K_{2/3}(y) - \mathrm{Int}K_{1/3}(y)}. \quad (5)$$

From Fig. 2(d) one can see that the linear polarization of the photon increases from 50% to 69% at an energy of 1 GeV and then decreases slowly. When $u \ll 1$, $\mathrm{Int}K_{1/3}(y) \ll K_{2/3}(y)$ and $\overline{\xi_3} \approx \frac{1}{2}$. As u increases, $\mathrm{Int}K_{1/3}(y)/K_{2/3}(y)$ increases rapidly, resulting in an increase in $\overline{\xi_3}$. According to Eq. (5), when u is larger than 0.7, $\mathrm{Int}K_{1/3}(y) \approx 0.9K_{2/3}(y)$ and $\overline{\xi_3} \approx \frac{1}{\frac{u^2-2u+2}{1-u} - 0.9} = \frac{1-u}{u^2-1.1u+1.1}$, which is very close to our simulation shown in Fig. 2(d). This figure shows that the high-energy photons tend to have low polarization and these photons usually distribute in small $|\theta_x|$ and $|\theta_y|$ as observed in Fig. 2(b). High-energy photons are mainly produced by high-energy electrons distributed in small $|\theta_x|$ and $|\theta_y|$. Low-energy photons distributed in large $|\theta_x|$ and $|\theta_y|$ have higher degrees of polarization whose parent electrons radiate strongly and lose substantial energy.

C. Influence of beam parameters

In Fig. 3, the influences of the length l_d of the driving beam on the photon number N_γ, photon polarization $\langle\xi_3\rangle$, and energy conversion efficiency η under different beam widths σ_d are studied, where the charge of the driving beam Q_d is 4 nC and $\sigma_s/\sigma_d = 0.5$. Comparing different lines in Fig. 3(a) shows that the photon number increases with the decrease of the driving beam width σ_d since a smaller σ_d causes a larger χ_e [see Eq. (2)] and consequently a higher radiation probability. This figure also displays that the photon number N_γ increases with the increase of l_d, since $N_\gamma \sim \frac{l_d}{c}\int du \frac{d^2W_{\mathrm{rad}}}{dudt}$, where $\frac{d^2W_{\mathrm{rad}}}{dudt}$ is the probability of radiation per unit of time per unit of energy. The photon number $N_\gamma \propto l_d^{1/3}$ at $\chi_e \gg 1$ and $N_\gamma \propto 1$ at $\chi_e \ll 1$, where the probability of radiation $\frac{dW_{\mathrm{rad}}}{dt}$ is inversely proportional to $l_d^{2/3}$ and l_d in the two cases [34], respectively. Note that for the longer l_d, the average energy of photons tends to decrease since χ_e is smaller according to Eq. (2). As shown in Fig. 3(c), energy conversion η decreases with the increase of l_d and σ_d, because the radiation energy of an electron is mainly determined by χ_e, which is inversely proportional to l_d and σ_d. Note that the reduction of η and the increase of N_γ with the growing l_d means that the average photon energy and the proportion of high-energy photons are reduced.

In Fig. 3(b), one can see that the average polarization of photons increases with the increase of l_d and σ_d. By summing the photon energy spectrum, one can obtain the expression of the total linear polarization of photons

$$\langle\xi_3\rangle = \frac{6\int_0^\infty dv \frac{\exp(-f)}{(1+v)^2} fv(4+3v-fv)}{\int_0^\infty dv \frac{\exp(-f)}{(1+v)^3} fv[3+29(1+v)^2 - 3fv(2+v) + f^2v^2]}, \quad (6)$$

where v is the integral variable and $f = v[3(1+v)]^{1/2}/\chi_e$; more details can be found in Appendix A. In Eq. (6), $\langle\xi_3\rangle$ decreases monotonically with χ_e (see Fig. 8 in Appendix A). According to Eq. (2), χ_e is inversely proportional to l_d and σ_d, so the average polarization of photons increases with the increase of l_d and σ_d.

Figure 4 shows the influence of the initial energy of the seeding electron beam on the photon number N_γ, photon polarization $\langle\xi_3\rangle$, and energy conversion efficiency η. Increasing the seeding beam energy ε_{s0} results in the reduction of the photon number and polarization as shown in Figs. 4(a) and 4(b), respectively. We notice that the increase of ε_{s0} has a slight effect on the photon number, e.g., the number of photons does not change by more than 5% when ε_{s0} is increased from 1 GeV to 10 GeV with $Q_d = 4$ nC. This can be explained by Eq. (3), which shows that W_{rad} is inversely

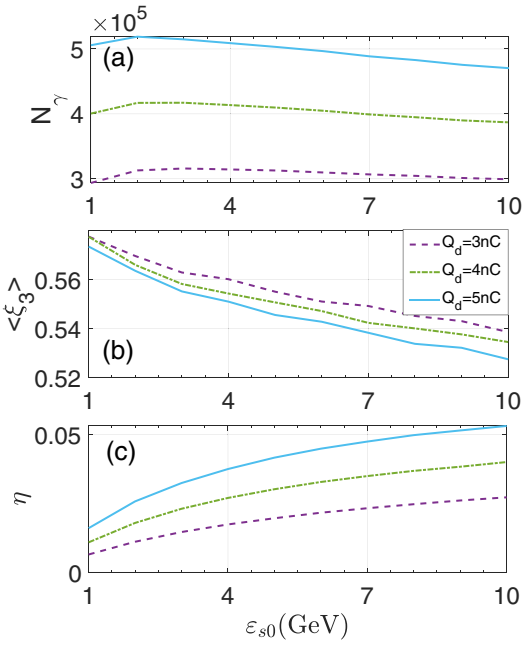

FIG. 4. (a) Photon number N_γ, (b) photon polarization $\langle\xi_3\rangle$, and (c) energy conversion efficiency η versus the seeding beam initial energy ε_{s0} in three cases with charges of the driving beam of Q_d = 3 nC (purple dashed line), 4 nC (green dash-dotted line), and 5 nC (cyan solid line), respectively.

proportional to the electron energy ε_e, which offsets the effect of the increase of χ_e. Increasing ε_{s0} leads to the increase in χ_e and the decrease in $\langle\xi_3\rangle$, in terms of Eq. (6) and the discussion above. In Fig. 4(c) it is found that increasing the seeding beam energy can improve the energy conversion efficiency as well as grow the proportion of high-energy photons. This is because $\eta \propto \int du\varepsilon_\gamma \frac{d^2W_{\rm rad}}{dudt} = \int du \frac{\alpha m^2c^4}{4\sqrt{3}\pi\hbar} u[\frac{u^2-2u+2}{1-u}K_{2/3}(y) - {\rm Int}K_{1/3}(y)] = \int du \frac{\alpha m^2c^4}{4\sqrt{3}\pi\hbar} u[\frac{u^2}{1-u}K_{2/3}(y) + {\rm Int}K_{5/3}(y)]$, and $K_{2/3}$ and ${\rm Int}K_{5/3}$ increase with the decrease of y, which is inversely proportional to ε_{s0}.

Increasing the charge of the driving beam Q_d also causes the growth of N_γ but the decrease of $\langle\xi_3\rangle$. This is because with the increase of χ_e as Q_d grows, N_γ goes up and $\langle\xi_3\rangle$ goes down [according to Eq. (6)]. One can increase the number of photons and the energy conversion efficiency by increasing Q_d according to Figs. 4(a) and 4(b). Meanwhile, the increased Q_d has a slight negative impact on the photon polarization.

D. Improving photon polarization through initial polarization of the seeding beam

Above we have taken an initially unpolarized seeding electron beam, and the polarization of the photons in the high-energy tail is relatively low, as shown in Fig. 2(d). To improve the polarization of high-energy photons, one can use a prepolarized seeding beam with a polarization along the y axis (or a transverse polarization), i.e., the spin direction of the electrons is the same as or opposite to the direction of the experienced effective magnetic field in the electron rest frame.

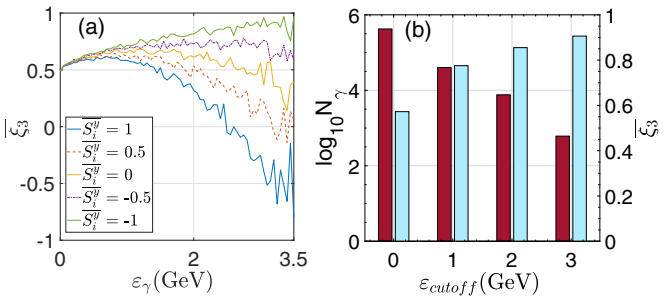

FIG. 5. (a) Photon polarization $\overline{\xi_3}$ versus photon energy ε_γ with various initial electron polarizations (from top to bottom) $\overline{S_i^y} = -1$ (green solid line), -0.5 (purple dash-dotted line), 0 (yellow solid line), 0.5 (orange dashed line), and 1 (blue solid line). (b) Photon number N_γ (left red bar) and average photon polarization $\overline{\xi_3}$ (right blue bar) versus the cutoff energy ε_γ.

The average polarization is given by Eq. (4). The first term

$$\frac{K_{2/3}(y)}{\frac{u^2-2u+2}{1-u}K_{2/3}(y) - {\rm Int}K_{1/3}(y) - uK_{1/3}(y)(\vec{S}_i\cdot\vec{e}_2)} \tag{7}$$

degenerates to $\frac{K_{2/3}(y)}{\frac{u^2-2u+2}{1-u}K_{2/3}(y)-{\rm Int}K_{1/3}(y)}$ in the case with an initially unpolarized seeding beam and it decays to 0 as u increases, which leads to low polarization of the high-energy photons. The second term of Eq. (4),

$$\frac{\frac{u}{1-u}K_{1/3}(y)(\vec{S}_i\cdot\vec{e}_2)}{\frac{u^2-2u+2}{1-u}K_{2/3}(y) - {\rm Int}K_{1/3}(y) - uK_{1/3}(y)(\vec{S}_i\cdot\vec{e}_2)}, \tag{8}$$

determines the polarization of high-energy photons, where $\frac{u}{1-u}K_{1/3}(y)$ increases monotonically with u and takes the maximum value around $u = 1$. When $\vec{S}_i\cdot\vec{e}_2 < 0$, $\overline{\xi_3}$ will increase towards 1 as photon energy increases, and when $\vec{S}_i\cdot\vec{e}_2 > 0$, $\overline{\xi_3}$ will decrease towards -1, which suggests that a prepolarized seeding beam can generate highly polarized photons with high energies.

In Fig. 5(a) we draw the photon polarization distribution when the initial polarization of the seeding beam $\overline{S_i^y} = -1$, -0.5, 0, 0.5, and 1. The average polarizability of the generated photons is 0.57, 0.56, 0.55, 0.54, and 0.53, respectively. For high-energy photons with energies higher than 3.5 GeV, $\overline{\xi_3} = 0.94$, 0.69, 0.35, -0.05, and -0.80, respectively. It is found that when $\overline{S_i^y} = 1$ (the electron spins are in the same direction as the magnetic field), $\overline{\xi_3}$ will first increase from about 0.5 and then decrease to -1 as the photon energy increases. If the electron spins are in the opposite direction to the magnetic field with $\overline{S_i^y} = -1$, $\overline{\xi_3}$ increases from about 0.5 to 1 as photon energy increases, so the average polarization is higher than the case with $\overline{S_i^y} = 1$. These results agree with Eq. (4) [the corresponding calculation of this equation is shown in Fig. 7(a)]. When a classical electromagnetic wave is radiated, the linear polarization $\overline{\xi_3}$ of the electromagnetic wave increases from 0.5 to about 1 with the increase of the electromagnetic wave frequency or photon energy [30]. This can explain why the photon polarization first increases from 0.5 with the photon energy at the low-energy range. While the photon energy is large enough, the quantum effect starts to

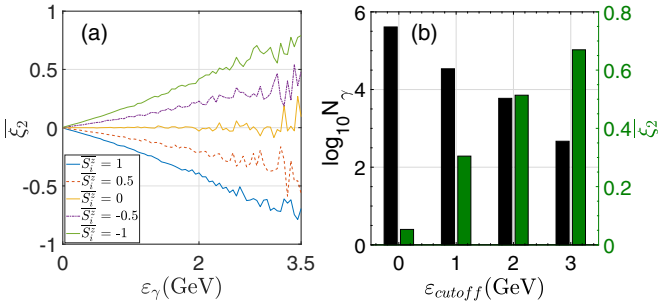

FIG. 6. (a) Photon polarization $\overline{\xi_2}$ versus photon energy ε_γ under various initial electron polarizations (from top to bottom) $\overline{S_i^z} = -1$ (green solid line), -0.5 (purple dash-dotted line), 0 (yellow solid line), 0.5 (orange dashed line), and 1 (blue solid line). (b) Photon number N_γ (left black bar) and average photon polarization $\overline{\xi_2}$ (right green bar) versus the cutoff energy ε_γ.

work, i.e., the electron spin will influence the photon polarization. When the electron spin is antiparallel to the magnetic field, $\overline{\xi_3}$ will increase to 1, as shown in the case with the initial electron spin of $\overline{S_i^y} = -1$ in Fig. 7(a). When the electron spin is parallel to the magnetic field, $\overline{\xi_3}$ decreases to -1, as shown in the case with the initial electron spin of $\overline{S_i^y} = 1$ in Fig. 7(a). When the electron is unpolarized (half with $\overline{S_i^y} = -1$ and half with $\overline{S_i^y} = 1$), $\overline{\xi_3}$ decreases to 0, as shown in the case with the initial electron spin of $\overline{S_i^y} = 0$ in Fig. 7(a). The other cases are intermediate states with the initial electron spin of $\overline{S_i^y} = 0.5$ and $\overline{S_i^y} = -0.5$ in Fig. 7(a).

In Fig. 5(b) we plot the number and polarizability of high-energy photons at different energy cutoff $\varepsilon_{\text{cutoff}}$, where we counted the photons with energy above $\varepsilon_{\text{cutoff}}$. With the increase of $\varepsilon_{\text{cutoff}}$, the number of photons is decreased and the photon polarization is increased, e.g., 0.15% of photons have energies over 3 GeV, but their average polarization can reach 90%. By contrast, the polarization is 43% when the seeding beam is unpolarized initially. The number ratios of the photons with energies over 1 and 2 GeV are 9.6% and 1.8% and the corresponding average polarizations are 78% and 86%, respectively.

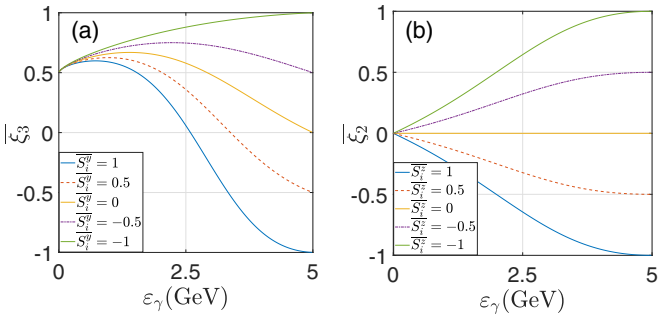

FIG. 7. (a) Linear photon polarization $\overline{\xi_3}$ versus photon energy ε_γ under various initial electron polarizations (from top to bottom) $\overline{S_i^y} = -1$ (green solid line), -0.5 (purple dash-dotted line), 0 (yellow solid line), 0.5 (orange dashed line), and 1 (blue solid line). (b) Circular photon polarization $\overline{\xi_2}$ versus photon energy ε_γ under various initial electron polarizations (from top to bottom) $\overline{S_i^z} = -1$ (green solid line), -0.5 (purple dash-dotted line), 0 (yellow solid line), 0.5 (orange dashed line), and 1 (blue solid line). Here $\chi_e = 0.38$ is taken, which is close to the typical value obtained in our simulation.

Next we proceed to study the generation of circularly polarized γ photons, which is related to the longitudinal polarization of the seeding beam. The circular polarization of photons can be written as

$$\overline{\xi_2} = (\vec{S}_i \cdot \vec{e}_v) \frac{\frac{2u-u^2}{1-u} K_{2/3}(y) - u\,\text{Int}K_{1/3}(y)}{\frac{u^2-2u+2}{1-u} K_{2/3}(y) - \text{Int}K_{1/3}(y)}, \tag{9}$$

and it is shown that a longitudinally prepolarized seeding beam with $\vec{S}_i \cdot \vec{e}_v \neq 0$ is necessary to achieve nonzero $\overline{\xi_2}$. Figure 6(a) shows the influence of the initial polarization of the seeding beam on the circular polarization of the generated γ photons. If an initially unpolarized electron beam is used, no circularly polarized photons can be produced, as observed in the line with $\overline{S_i^z} = 0$ in Fig. 6(a). Left-handed circularly polarized photons can be produced when the spin direction of the electron is along its movement direction. Right-handed circularly polarized photons can be produced when these two directions are opposite. With an unpolarized beam, the numbers of the left-handed and right-handed circularly polarized photons are the same and they can be summed to linear polarized photons. If the seeding beam has initially longitudinal polarization with $\overline{S_i^z} = \pm 1$ and ± 0.5, circularly polarized photons can be obtained and the circular polarization grows with the increasing $|\overline{S_i^z}|$ [see Fig. 6(a)], where the average circular polarization is 5.3%, with $\overline{S_i^z} = -1$. The circular polarization grows with the increase of the photon energy, as shown in Fig. 6(a). In Fig. 6(b) we plot the circular polarization of photons in different photon energy cutoffs when $\overline{S_i^z} = -1$ is taken. As $\varepsilon_{\text{cutoff}}$ is increased from 1 GeV to 2 GeV and 3 GeV, the average circular polarization goes up from 30% to 51% and 67%, respectively. This suggests that the scheme with a longitudinally prepolarized seeding beam is favorable for generating high-energy circularly polarized photons with sufficiently high polarization.

We calculate the photon polarization with different initial polarizations of the seeding beam according to Eqs. (4) and (9) and present the results in Fig. 7. Figure 7(a) shows the linear photon polarization $\overline{\xi_3}$ with different initial electron polarization and Fig. 7(b) shows the circular photon polarization. One can see that the theoretical results are close to the simulation results present in Figs. 5(a) and 6(a) with different initial electron polarization. Note that $\overline{\xi_2}$ appears symmetric with distributions $\overline{S_i^z} = 1$ and $\overline{S_i^z} = -1$ as well as $\overline{S_i^z} = 0.5$ and $\overline{S_i^z} = -0.5$ since $\overline{\xi_2} \propto \vec{S}_i \cdot \vec{e}_v$, as shown in Eq. (9).

One can notice that $\overline{\xi_3}$ will increase towards 1 as the photon energy increases when $\overline{S_i^y} = -1$ and $\overline{\xi_3}$ will decrease towards -1 when $\overline{S_i^y} = 1$. In addition, $\overline{\xi_2}$ will increase towards 1 when $\overline{S_i^z} = -1$ and $\overline{\xi_1}$ will increase towards 1 when $\overline{S_i^x} = -1$. The spin quantum state of an electron can be represented by a point $(\overline{S_i^x}, \overline{S_i^y}, \overline{S_i^z})$ on the Bloch sphere. The average polarization of a photon can be represented by a point $(\overline{\xi_1}, \overline{\xi_3}, \overline{\xi_2})$ on the Poincaré sphere. One can see that there is a one-to-one correspondence between coordinate points on the spheres. Because

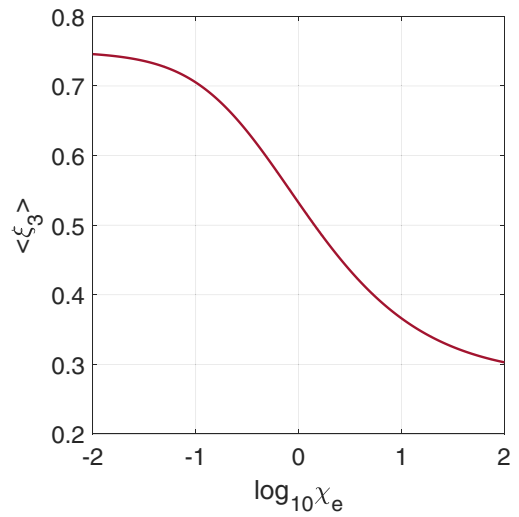

FIG. 8. Photon polarization $\langle\xi_3\rangle$ versus QED parameter χ_e.

of this one-to-one correspondence, one could expect that the electron polarization could be transferred to the photon polarization in the nonlinear Compton scattering process.

IV. CONCLUSION

Through a series of Monte Carlo simulations, it was found that a linearly polarized photon beam with an average polarization of 55% can be obtained by the collision of two unpolarized ultrarelativistic electron beams. Increasing the charge of the driving beam and decreasing the width of the driving beam could significantly increase the photon yield, with little effect on the photon polarization. When a prepolarized seeding beam was used, the photons with high energies could have a high polarization. For example, if the transverse polarization of the seeding beam was $\overline{S_i^y} = -1$, the average polarization of high-energy photons with energies greater than 3 GeV could reach 90%. Circularly polarized photons could be obtained by using an initially longitudinally polarized seeding beam and the average circular polarization of the photons with energy greater than 3 GeV could reach 67%.

ACKNOWLEDGMENTS

This work was supported by the Strategic Priority Research Program of Chinese Academy of Sciences (Grant No. XDA25050300), the National Key R&D Program of China (Grant No. 2018YFA0404801), and the Fundamental Research Funds for the Central Universities, the Research Funds of Renmin University of China (Grant No. 20XNLG01). Computational resources were provided by the Physical Laboratory of High Performance Computing at Renmin University of China.

APPENDIX A: DEPENDENCE OF ξ_3 ON χ_e

We derive the dependence of ξ_3 on χ_e. The radiation intensity matrix can be expressed as

$$\begin{aligned} dI_{12} &= dI_{21} = 0, \\ dI_{11} &= \frac{e^2m^2\zeta\,d\zeta}{2\sqrt{3}\pi\hbar^2(1+\eta)^3}\left[\int_{2\zeta/3\chi_e}^{\infty} K_{5/3}(y)dy + \left(1+\frac{\zeta^2}{1+\zeta}\right)K_{2/3}\left(\frac{2\zeta}{3\chi_e}\right)\right], \\ dI_{22} &= \frac{e^2m^2\zeta\,d\zeta}{2\sqrt{3}\pi\hbar^2(1+\zeta)^3}\left[\int_{2\zeta/3\chi_e}^{\infty} K_{5/3}(y)dy + \left(-1+\frac{\zeta^2}{1+\zeta}\right)K_{2/3}\left(\frac{2\zeta}{3\chi_e}\right)\right], \end{aligned} \tag{A1}$$

where $\zeta = \frac{\hbar\omega}{\varepsilon_e-\hbar\omega}$. Then we integrate over ζ and get the formula

$$\begin{aligned} I_e &= I_{11} + I_{22} \\ &= \frac{e^2m^2}{\sqrt{3}\pi\hbar^2}\int_0^{\infty}\frac{\zeta\,d\zeta}{(1+\zeta)^3}\left[\int_{2\zeta/3\chi_e}^{\infty} K_{5/3}(y)dy + \frac{\zeta^2}{1+\zeta}K_{2/3}\left(\frac{2\zeta}{3\chi_e}\right)\right] \\ &= \frac{e^2m^2}{3\sqrt{3}\pi\hbar^2}\int_0^{\infty}\frac{\zeta(4\zeta^2+5\zeta+4)}{(1+\zeta)^4}K_{2/3}\left(\frac{2\zeta}{3\chi_e}\right)d\zeta, \end{aligned} \tag{A2}$$

$$I_- = I_{11} - I_{22} = \frac{e^2m^2}{\sqrt{3}\pi\hbar^2}\int_0^{\infty}\frac{\zeta\,d\zeta}{(1+\zeta)^3}K_{2/3}\left(\frac{2\zeta}{3\chi_e}\right). \tag{A3}$$

Then we use the integral representation of the McDonald function

$$\int_{-\infty}^{\infty} x\sin(bx+ax^3)dx = \frac{2}{3\sqrt{3}}\frac{b}{a}K_{2/3}(\sigma), \tag{A4}$$

where $\sigma = (2/3\sqrt{3})(b^{3/2}/a^{1/2})$, and obtain

$$I_e = \frac{e^2m^2}{6\pi i\hbar^2}\int_0^{\infty}\frac{4\zeta^3+5\zeta^2+4\zeta}{(1+\zeta)^4}\int_{-\infty}^{\infty} d\tau\,\tau e^{i\zeta(\tau+\tau^3/3)/\chi_e}, \tag{A5}$$

$$I_- = \frac{e^2m^2}{2i\pi\hbar^2}\int_0^\infty \frac{\zeta}{(1+\zeta)^3}\int_{-\infty}^{\infty} d\tau\,\tau e^{i\zeta(\tau+\tau^3/3)/\chi_e}. \tag{A6}$$

Changing the variable $v = \zeta(1+\tau^2/3)$ and integrating over τ, we have

$$I_e = \frac{e^2m^2}{64\hbar^2}\int_0^\infty dv \frac{e^{-f}}{(1+v)^3} fv[3+29(1+v)^2 - 3fv(2+v) + f^2v^2], \tag{A7}$$

$$I_- = \frac{3e^2m^2}{16\hbar^2}\int_0^\infty dv \frac{e^{-f}}{(1+v)^2} fv(4+3v-fv), \tag{A8}$$

where $f = v\sqrt{3(1+v)}/\chi_e$. Finally, by summing the photon energy spectrum, we can obtain the total linear polarization of photons $\langle\xi_3\rangle$:

$$\langle\xi_3\rangle = \frac{I_-}{I_e} = \frac{12\int_0^\infty dv \frac{e^{-f}}{(1+v)^2} fv(4+3v-fv)}{\int_0^\infty dv \frac{e^{-f}}{(1+v)^3} fv[3+29(1+v)^2 - 3fv(2+v)+f^2v^2]}. \tag{A9}$$

The dependence of $\langle\xi_3\rangle$ on χ_e can be calculated according to Eq. (A9) and the result is shown in Fig. 8.

APPENDIX B: ANGLE-INTEGRATED RADIATION PROBABILITY

The angle-integrated radiation probability of a polarized photon with a polarized electron is

$$\begin{aligned}\frac{d^2W_\gamma}{dudt} = \frac{\alpha m^2c^4}{4\sqrt{3}\pi\hbar\varepsilon_e}\Bigg[&\frac{u^2-2u+2}{1-u}K_{2/3}(y) - \mathrm{Int}K_{1/3}(y) - uK_{1/3}(y)(\vec{S}_i\cdot\vec{e}_2) - \frac{u}{1-u}K_{\frac{1}{3}}(y)(\vec{S}_f\cdot\vec{e}_2)\\ &+[2K_{\frac{2}{3}}(y) - \mathrm{Int}K_{1/3}(y)](\vec{S}_i\cdot\vec{S}_f) + \frac{u^2}{1-u}[K_{2/3}(y)-\mathrm{Int}K_{1/3}(y)](\vec{S}_i\cdot\vec{e}_v)(\vec{S}_f\cdot\vec{e}_v) + \frac{u}{1-u}K_{1/3}(y)(\vec{S}_i\cdot\vec{e}_1)\xi_1\\ &+\left(\frac{2u-u^2}{1-u}K_{2/3}(y) - u\,\mathrm{Int}K_{1/3}(y)\right)(\vec{S}_i\cdot\vec{e}_v)\xi_2 + \left(K_{2/3}(y) - \frac{u}{1-u}K_{1/3}(y)(\vec{S}_i\cdot\vec{e}_2)\right)\xi_3\Bigg].\end{aligned} \tag{B1}$$

After summing the polarization of the photon, we get

$$\begin{aligned}\frac{d^2\overline{W_\gamma}}{dudt} = \frac{\alpha m^2c^4}{2\sqrt{3}\pi\hbar\varepsilon_e}\Bigg(&\frac{u^2-2u+2}{1-u}K_{2/3}(y) - \mathrm{Int}K_{1/3}(y) - uK_{1/3}(y)(\vec{S}_i\cdot\vec{e}_2) - \frac{u}{1-u}K_{1/3}(y)(\vec{S}_f\cdot\vec{e}_2)\\ &+[2K_{2/3}(y)-\mathrm{Int}K_{1/3}(y)](\vec{S}_i\cdot\vec{S}_f) + \frac{u^2}{1-u}[K_{2/3}(y)-\mathrm{Int}K_{1/3}(y)](\vec{S}_i\cdot\vec{e}_v)(\vec{S}_f\cdot\vec{e}_v)\Bigg).\end{aligned} \tag{B2}$$

Here we choose the fixed axis $\vec{v}\times\vec{a}$ as the spin quantization axis. After radiating a photon, the probabilities of the electron spin along $\vec{e}_2$ and $-\vec{e}_2$ are

$$\begin{aligned}\left.\frac{d^2\overline{W_\gamma}}{dudt}\right|_{\vec{S}_f=\vec{e}_2} = \frac{\alpha m^2c^4}{2\sqrt{3}\pi\hbar\varepsilon_e}\Bigg(&\frac{u^2-2u+2}{1-u}K_{2/3}(y) - \mathrm{Int}K_{1/3}(y) - uK_{1/3}(y)(\vec{S}_i\cdot\vec{e}_2) - \frac{u}{1-u}K_{1/3}(y)\\ &+[2K_{2/3}(y)-\mathrm{Int}K_{1/3}(y)](\vec{S}_i\cdot\vec{e}_2)\Bigg)\end{aligned} \tag{B3}$$

and

$$\begin{aligned}\left.\frac{d^2\overline{W_\gamma}}{dudt}\right|_{\vec{S}_f=-\vec{e}_2} = \frac{\alpha m^2c^4}{2\sqrt{3}\pi\hbar\varepsilon_e}\Bigg(&\frac{u^2-2u+2}{1-u}K_{2/3}(y) - \mathrm{Int}K_{1/3}(y) - uK_{1/3}(y)(\vec{S}_i\cdot\vec{e}_2) + \frac{u}{1-u}K_{1/3}(y)\\ &-[2K_{2/3}(y)-\mathrm{Int}K_{1/3}(y)](\vec{S}_i\cdot\vec{e}_2)\Bigg),\end{aligned} \tag{B4}$$

respectively.

[1] P. Laurent, J. Rodriguez, J. Wilms, M. C. Bel, K. Pottschmidt, and V. Grinberg, Polarized gamma-ray emission from the galactic black hole Cygnus X-1, Science **332**, 438 (2011).

[2] U. I. Uggerhøj, The interaction of relativistic particles with strong crystalline fields, Rev. Mod. Phys. **77**, 1131 (2005).

[3] G. Moortgat-Pick, T. Abe, G. Alexander, B. Ananthanarayan, A. Babich, V. Bharadwaj, D. Barber, A. Bartl, A. Brachmann, S. Chen, J. Clarke, J. Clendenin, J. Dainton, K. Desch, M. Diehl, B. Dobos, T. Dorland, H. Dreiner, H. Eberl, J. Ellis *et al.*, Polarized positrons and electrons at the linear collider, Phys. Rep. **460**, 131 (2008).

[4] J. K. Koga and T. Hayakawa, Possible precise measurement of Delbrück scattering using polarized photon beams, Phys. Rev. Lett. **118**, 204801 (2017).

[5] T.-T. Qin, W. Luo, H.-Y. Lan, and W.-M. Wang, Ultrafast probing of plasma ion temperature in proton–boron fusion by nuclear resonance fluorescence emission spectroscopy, Matter Radiat. Extremes **7**, 035901 (2022).

[6] A. V. Subashiev, Y. A. Mamaev, Y. P. Yashin, and J. E. Clendenin, Spin polarized electrons: Generation and applications, Phys. Low Dimen. Struct. **1**, 1 (1999).

[7] T. Omori, M. Fukuda, T. Hirose, Y. Kurihara, R. Kuroda, M. Nomura, A. Ohashi, T. Okugi, K. Sakaue, T. Saito, J. Urakawa, M. Washio, and I. Yamazaki, Efficient propagation of polarization from laser photons to positrons through Compton scattering and electron-positron pair creation, Phys. Rev. Lett. **96**, 114801 (2006).

[8] G. Alexander, J. Barley, Y. Batygin, S. Berridge, V. Bharadwaj, G. Bower, W. Bugg, F.-J. Decker, R. Dollan, Y. Efremenko, V. Gharibyan, C. Hast, R. Iverson, H. Kolanoski, J. Kovermann, K. Laihem, T. Lohse, K. T. McDonald, A. A. Mikhailichenko, G. A. Moortgat-Pick *et al.*, Observation of polarized positrons from an undulator-based source, Phys. Rev. Lett. **100**, 210801 (2008).

[9] V. Petrillo, A. Bacci, C. Curatolo, I. Drebot, A. Giribono, C. Maroli, A. R. Rossi, L. Serafini, P. Tomassini, C. Vaccarezza, and A. Variola, Polarization of x-gamma radiation produced by a Thomson and Compton inverse scattering, Phys. Rev. ST Accel. Beams **18**, 110701 (2015).

[10] H. Olsen and L. C. Maximon, Photon and electron polarization in high-energy bremsstrahlung and pair production with screening, Phys. Rev. **114**, 887 (1959).

[11] D. Abbott, P. Adderley, A. Adeyemi, P. Aguilera, M. Ali, H. Areti, M. Baylac, J. Benesch, G. Bosson, B. Cade, A. Camsonne, L. S. Cardman, J. Clark, P. Cole, S. Covert, C. Cuevas, O. Dadoun, D. Dale, H. Dong, J. Dumas *et al.* (PEPPo Collaboration), Production of highly polarized positrons using polarized electrons at MeV energies, Phys. Rev. Lett. **116**, 214801 (2016).

[12] S. Tang, B. King, and H. Hu, Highly polarised gamma photons from electron-laser collisions, Phys. Lett. B **809**, 135701 (2020).

[13] Y.-Y. Chen, K. Z. Hatsagortsyan, C. H. Keitel, and R. Shaisultanov, Electron spin- and photon polarization-resolved probabilities of strong-field QED processes, Phys. Rev. D **105**, 116013 (2022).

[14] Y.-Y. Chen, P.-L. He, R. Shaisultanov, K. Z. Hatsagortsyan, and C. H. Keitel, Polarized positron beams via intense two-color laser pulses, Phys. Rev. Lett. **123**, 174801 (2019).

[15] K. Xue, Z.-K. Dou, F. Wan, T.-P. Yu, W.-M. Wang, J.-R. Ren, Q. Zhao, Y.-T. Zhao, Z.-F. Xu, and J.-X. Li, Generation of highly-polarized high-energy brilliant γ-rays via laser-plasma interaction, Matter Radiat. Extremes **5**, 054402 (2020).

[16] Y.-F. Li, R. Shaisultanov, Y.-Y. Chen, F. Wan, K. Z. Hatsagortsyan, C. H. Keitel, and J.-X. Li, Polarized ultrashort brilliant multi-GeV γ rays via single-shot laser-electron interaction, Phys. Rev. Lett. **124**, 014801 (2020).

[17] A. Di Piazza, C. Müller, K. Z. Hatsagortsyan, and C. H. Keitel, Extremely high-intensity laser interactions with fundamental quantum systems, Rev. Mod. Phys. **84**, 1177 (2012).

[18] V. M. Biryukov, Y. A. Chesnokov, and V. I. Kotov, *Crystal Channeling and its Application at High-Energy Accelerators* (Springer Science+Business Media, New York, 2013).

[19] C. Danson, D. Hillier, N. Hopps, and D. Neely, Petawatt class lasers worldwide, High Power Laser Sci. Eng. **3**, e3 (2015).

[20] J. W. Yoon, Y. G. Kim, I. W. Choi, J. H. Sung, H. W. Lee, S. K. Lee, and C. H. Nam, Realization of laser intensity over 10^{23} W/cm^2, Optica **8**, 630 (2021).

[21] W.-M. Wang, Z.-M. Sheng, P. Gibbon, L.-M. Chen, Y.-T. Li, and J. Zhang, Collimated ultrabright gamma rays from electron wiggling along a petawatt laser-irradiated wire in the QED regime, Proc. Natl. Acad. Sci. USA **115**, 9911 (2018).

[22] X.-L. Zhu, M. Chen, S.-M. Weng, T.-P. Yu, W.-M. Wang, F. He, Z.-M. Sheng, P. McKenna, D. A. Jaroszynski, and J. Zhang, Extremely brilliant GeV γ-rays from a two-stage laser-plasma accelerator, Sci. Adv. **6**, eaaz7240 (2020).

[23] F. Del Gaudio, T. Grismayer, R. A. Fonseca, W. B. Mori, and L. O. Silva, Bright γ rays source and nonlinear Breit-Wheeler pairs in the collision of high density particle beams, Phys. Rev. Accel. Beams **22**, 023402 (2019).

[24] V. Yakimenko, S. Meuren, F. Del Gaudio, C. Baumann, A. Fedotov, F. Fiuza, T. Grismayer, M. J. Hogan, A. Pukhov, L. O. Silva, and G. White, Prospect of studying nonperturbative QED with beam-beam collisions, Phys. Rev. Lett. **122**, 190404 (2019).

[25] R. J. Noble, Beamstrahlung from colliding electron-positron beams with negligible disruption, Nucl. Instrum. Methods Phys. Res. Sect. A **256**, 427 (1987).

[26] A. Sampath, X. Davoine, S. Corde, L. Gremillet, M. Gilljohann, M. Sangal, C. H. Keitel, R. Ariniello, J. Cary, H. Ekerfelt, C. Emma, F. Fiuza, H. Fujii, M. Hogan, C. Joshi, A. Knetsch, O. Kononenko, V. Lee, M. Litos, K. Marsh *et al.*, Extremely dense gamma-ray pulses in electron beam-multifoil collisions, Phys. Rev. Lett. **126**, 064801 (2021).

[27] N. V. Elkina, A. M. Fedotov, I. Y. Kostyukov, M. V. Legkov, N. B. Narozhny, E. N. Nerush, and H. Ruhl, QED cascades induced by circularly polarized laser fields, Phys. Rev. ST Accel. Beams **14**, 054401 (2011).

[28] C. Ridgers, J. Kirk, R. Duclous, T. Blackburn, C. Brady, K. Bennett, T. Arber, and A. Bell, Modelling gamma-ray photon emission and pair production in high-intensity laser–matter interactions, J. Comput. Phys. **260**, 273 (2014).

[29] A. Gonoskov, S. Bastrakov, E. Efimenko, A. Ilderton, M. Marklund, I. Meyerov, A. Muraviev, A. Sergeev, I. Surmin, and E. Wallin, Extended particle-in-cell schemes for physics in ultrastrong laser fields: Review and developments, Phys. Rev. E **92**, 023305 (2015).

[30] V. N. Baier, V. M. Katkov, and V. M. Strakhovenko, *Electromagnetic Processes at High Energies in Oriented Single Crystals* (World Scientific, Singapore, 1998).

[31] Y.-F. Li, Y.-Y. Chen, W.-M. Wang, and H.-S. Hu, Production of highly polarized positron beams via helicity transfer from polarized electrons in a strong laser field, Phys. Rev. Lett. **125**, 044802 (2020).

[32] H.-H. Song, W.-M. Wang, and Y.-T. Li, Generation of polarized positron beams via collisions of ultrarelativistic electron beams, Phys. Rev. Res. **3**, 033245 (2021).

[33] A. Gonoskov, T. G. Blackburn, M. Marklund, and S. S. Bulanov, Charged particle motion and radiation in strong electromagnetic fields, Rev. Mod. Phys. **94**, 045001 (2022).

[34] V. B. Berestetskii, E. M. Lifshitz, and L. P. Pitaevskii, *Quantum Electrodynamics* (Butterworth-Heinemann, Oxford, 1982), Vol. 4.

[35] V. I. Ritus, Quantum effects of the interaction of elementary particles with an intense electromagnetic field, J. Sov. Laser Res. **6**, 497 (1985).

[36] A. Di Piazza, M. Tamburini, S. Meuren, and C. H. Keitel, Implementing nonlinear Compton scattering beyond the local-constant-field approximation, Phys. Rev. A **98**, 012134 (2018).

[37] A. Di Piazza, M. Tamburini, S. Meuren, and C. H. Keitel, Improved local-constant-field approximation for strong-field QED codes, Phys. Rev. A **99**, 022125 (2019).

[38] A. Ilderton, B. King, and D. Seipt, Extended locally constant field approximation for nonlinear Compton scattering, Phys. Rev. A **99**, 042121 (2019).

[39] T. Podszus and A. Di Piazza, High-energy behavior of strong-field QED in an intense plane wave, Phys. Rev. D **99**, 076004 (2019).

[40] Y.-F. Li, R. Shaisultanov, K. Z. Hatsagortsyan, F. Wan, C. H. Keitel, and J.-X. Li, Ultrarelativistic electron-beam polarization in single-shot interaction with an ultraintense laser pulse, Phys. Rev. Lett. **122**, 154801 (2019).

[41] V. Bargmann, L. Michel, and V. L. Telegdi, Precession of the polarization of particles moving in a homogeneous electromagnetic field, Phys. Rev. Lett. **2**, 435 (1959).

[42] V. Yakimenko, L. Alsberg, E. Bong, G. Bouchard, C. Clarke, C. Emma, S. Green, C. Hast, M. J. Hogan, J. Seabury, N. Lipkowitz, B. O'Shea, D. Storey, G. White, and G. Yocky, FACET-II facility for advanced accelerator experimental tests, Phys. Rev. Accel. Beams **22**, 101301 (2019).

[43] A. Pukhov and J. P. Farmer, Stable particle acceleration in coaxial plasma channels, Phys. Rev. Lett. **121**, 264801 (2018).